ACS Photonics

pubs.acs.org/journal/apchd5

Article

Generalized Modular Spectrometers Combining a Compact Nanobeam Microcavity and Computational Reconstruction

Ziwei Cheng, Yuhe Zhao, Jiahui Zhang, Hailong Zhou, Dingshan Gao, Jianji Dong,* and Xinliang Zhang

Cite This: https://doi.org/10.1021/acsphotonics.1c00719

Read Online

ACCESS | Metrics & More | Article Recommendations | Supporting Information

ABSTRACT: Compact and integrated spectrometers are sought after with great effort for the applications of portable spectroscopy devices and lab-on-a-chip systems. Material engineered spectrometers exhibited superior performances in terms of their compact footprint and high resolution after assistance by computational reconstruction but were still hindered by low yield, poor scalability, and poor transplantation to other frequency bands. Here we propose a structure engineered spectrometer based on an ultracompact photonic crystal nanobeam cavity (PCNC) array with computational reconstruction. The spectrometer shows a compact footprint, good scalability and good transplantability simultaneously. We fabricate the PCNC structure on a silicon-on-insulator chip and demonstrate the reconstruction of incident-light spectra around 1580 nm with the measured powers of the nanobeam filter array. The spectrometer is proven to be easily transplanted to other operation bands, such as 1310 and 2400 nm. With the advantages of high yield fabrication and structure flexibility, this PCNC spectrometer can be easily customized as a generalized modular solution to realize various commercial spectrometer products for different spectroscopy bands.

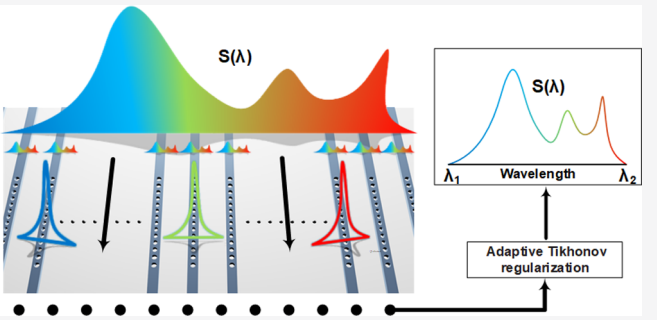

KEYWORDS: *spectrometer, computational reconstruction, photonic crystals, nanobeam cavity*

Spectrometers are ubiquitous analytical tools of optics in many fields from fundamental scientific research to industrial applications such as astrophotonics, earth sciences, precision agriculture, and clinical and chemical analysis.[1−4] The increasing demands for portable and low-cost devices and lab-on-a-chip systems have fostered the development of miniaturized and integrated spectrometers with comparable spectral resolutions.[5−16] Most microspectrometers are realized by miniaturizing the diffractive optics or interference filters from conventional bulky spectrometers with integrated optical technology.[7,17−26] However, the long optical path length of diffractive elements leads to a relatively large footprint to accumulate a detectable phase difference for high resolution.[27−34] Although resonant filters such as film filters[17] and integrated microrings[18,35−37] can reduce the path length, it is difficult to precisely control the resonant wavelength in fabrication as the requirement of the narrowband filter spectrometers. Besides, the operating wavelength range would be limited by the free spectral range (FSR) of these filters.

Photonic crystal (PhC) filters on two-dimensional dielectric slabs are suitable to act as the compact basic unit for microspectrometers due to the flexible structure engineering and excellent performance on control and confinement of light.[38−44] A photonic crystal nanobeam cavity (PCNC) further greatly reduces the footprint of the photonic crystal slab to a one-dimension narrow beam while preserving the ability of strong light confinement.[45−50] The photonic bandgap engineering and mode volume compressing enable the single band-pass filter feature in a large operating wavelength range as well as the prominent cavity footprint among integrated filters. However, those compact narrowband filters have low yield in massive production because of the fabrication sensitivity to the high Q factor and resonant frequency.

Most recently, the rise of computational spectral reconstruction methods has promoted the development of miniature spectrometers by circumventing the strict filtering constraints.[51,52] The precalibration of spectrum mapping from input channel to output array offers more tolerance in structure and material selection, bringing out novel spectrometers based on disordered structure,[53] random PhC slabs,[42] quantum dots (QDs)[54,55] and single nanowires.[56] The on-chip disordered structure proposed by Redding et al. implemented multiple light scattering, enabling high resolution with a small footprint.[53] The PhC slab array with different random responsivities demonstrated by Wang et al. realized a single-

Received: May 14, 2021

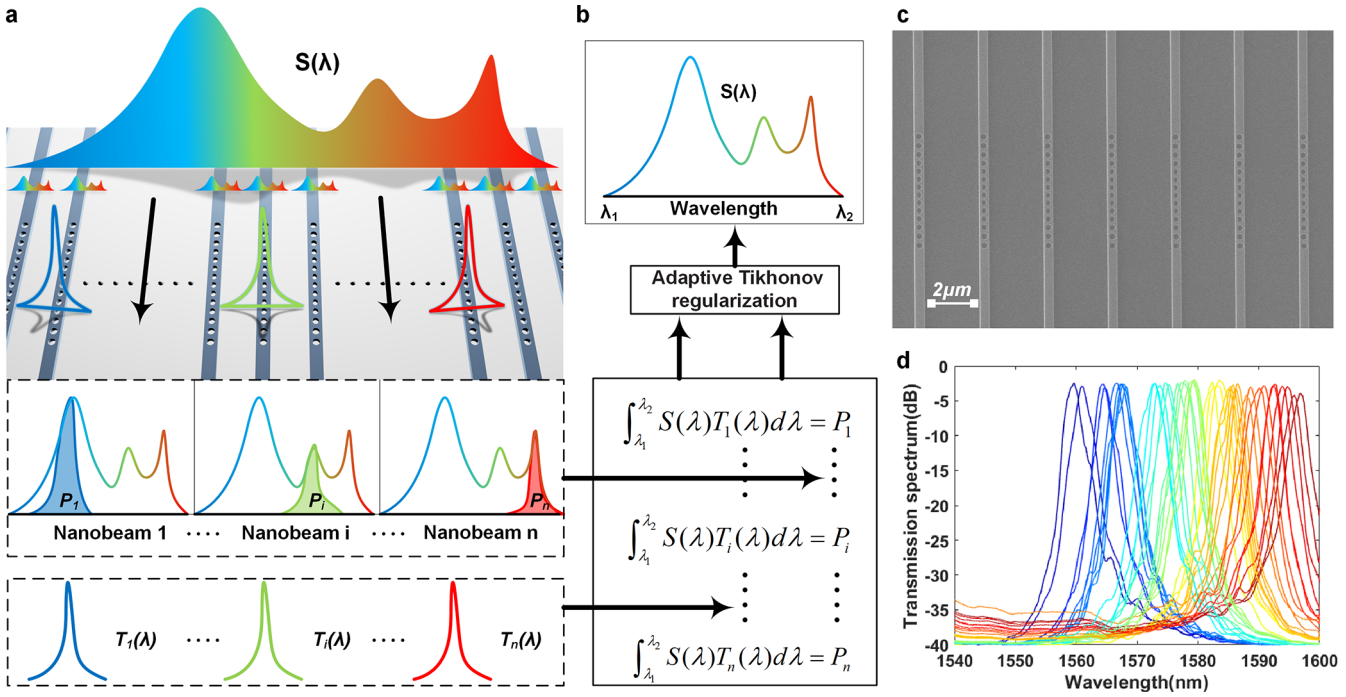

Figure 1. Operational schematic and characterization of the PCNC array spectrometer. (a) Receiving and response process of the PCNC spectrometer to arbitrary spectrum incident-light: schematic incident process (top), transmitted intensities (middle), and transmission functions (bottom). (b) Computational reconstruction process. Mathematical description of the receiving and response process of PCNC spectrometer (bottom), solving method for the equation set (middle), and reconstructed spectrum of the incident light (top). (c) SEM image of fabricated PCNC spectrometer SOI chip. There is only a 3 μm distance between each PCNC unit. Scale bar: 2 μm. (d) Normalized spectral transmission of each filter unit in the PCNC spectrometer.

shot spectrometer with high resolution and low cost.[42] By using continuously tunable and broadband CdSe QDs or CdS QDs, Bao and Bawendi illustrated a convenient QD spectrometer for the whole visible range.[54] And, Yang et al. showed an extremely compact spectrometer only as a single nanowire by the composition-gradient alloying method.[56] These computational spectrometers paved the way for accurate reconstruction of spectra across visible and infrared bands with extra small footprints and simplified structures. However, with nonstandard structures with random responsivities, it may be difficult to keep resolution uniformity. Finely tuned-material-based spectrometers such as QDs and nanowires still face some challenges with respect to fabrication complexity and transfer difficulty for integration and stability. Fortunately, structure engineered photonic devices such as PCNC can benefit from the complementary metal oxide semiconductor (CMOS) compatible fabrication process.

In this work, we demonstrate a structure engineered spectrometer by combining the advantages of a continuously tunable PCNC dense array and computational spectral reconstruction method. The PCNC units are densely arrayed with an only 6 μm core length and a 3 μm distance, forming a compact footprint of the whole spectrometer. The number of PCNCs could be easily increased with the demand for higher resolution or broader operating bandwidth. Compared with the material based computational spectrometers, the PCNC spectrometer not only has advantages in terms of fabrication and integration with the CMOS compatible process but also can be transplanted to other wavelength ranges due to the correlation between the operating frequency and lattice size of PhC.[42,44] We achieve accurate reconstruction of spectra around 1580 nm with an extinction ratio up to 30 dB and transplant the spectrometer to near 1310 and 2400 nm by simply scaling the size parameters of the prototype. The generalized modular PCNC spectrometer shows promising potential to construct commercial spectrometer products for applications in wideband scenarios through an agile customization flow.

RECONSTRUCTION PRINCIPLE

Figure 1a schematically describes the operating process and principle of the PCNC spectrometer. The unknown incident light, whose spectrum is defined as function $S(\lambda)$ (where λ is wavelength), passes through the horizontally aligned PCNC filters from top to bottom. The colored Lorentzian line shape above a certain PCNC filter represents the transmission spectrum of this filter with different resonant wavelengths. The corresponding transmission functions are calibrated as $T_i(\lambda)$ (where i = 1, 2, ... n is the PCNC serial number) in advance. A set of transmitted intensities are measured after the PCNC units as P_i, as shown in middle of Figure 1a. The intensity is the integral of incident-light spectrum and transmission function of each PCNC with respect to wavelength. The $S(\lambda)$ could be reconstructed by solving a system of linear equations of this process:

$$\int_{\lambda_1}^{\lambda_2} S(\lambda)T_i(\lambda)\,\mathrm{d}\lambda = P_i \quad (i = 1, 2, 3 \ldots, n) \tag{1}$$

where λ_1 and λ_2 define the operating wavelength range of the spectrometer. Figure 1b illustrates the computational reconstruction process based on the precalibrated $T_i(\lambda)$ and measured P_i. Considering the inconsistencies of the equations introduced by the measurement errors in both $T_i(\lambda)$ and P_i, the iterative regression method is needed to obtain

https://doi.org/10.1021/acsphotonics.1c00719
ACS Photonics XXXX, XXX, XXX−XXX

approximate solutions.[57] Here we apply adaptive Tikhonov regularization algorithm to further reduce the instability of overfitting, which uses a linear combination of Gaussian basic functions to fit the target spectrum[56,58] [see Supplement 1].

Without loss of generality, we design and fabricate a universal PCNC arrayed spectrometer on a silicon-on-insulator (SOI) platform due to its small size, fabrication maturity, low cost in massive production, and applicability for Telecom Band.[59] This spectrometer scheme is also suitable for other integrated platforms as long as the material is low-loss to the target wavelength range such as ultraviolet light, visible light, and mid-infrared light. As shown in the scanning electron microscope (SEM) image in Figure 1c, the one-dimension waveguide shape and low sidewall power leakage enable the dense arrangement of PCNC units on the other dimension by 3 μm spacing, contributing to the compact footprint of the whole spectrometer. The close distance can effectively reduce the fabrication errors between two adjacent PCNC units. Therefore, the fabrication errors would only reduce the Q factor of PCNCs which results in a relatively broadband filter but does not affect the gradual change among PCNC resonance, which is an exactly suitable feature for the computational reconstruction method. There are 38 PCNC units in the spectrometer, which can be flexibly increased or decreased with the requirements of resolution or operating spectrum range. The calibrated transmission spectra of the 38 PCNC units are shown in Figure 1d. Note that we used same grating coupler structures for the input and output of each unit, which can basically ensure the consistency. The deviation introduced is included in the transmission spectra, and it can be compensated by computational reconstruction algorithms. If on-chip spectrum measurement is required, a beam splitter can be introduced for the input light of each unit. As we can see, the central resonant wavelength of each PCNC is slightly shifted and gradually changed while the line shape of the transmission spectrum remains consistent. Note that this feature can optimize the consistency of resolution to a certain extent, and a more uniformly distributed transmission line shape is expected to ensure better consistency.

DEVICE DESIGN

Figure 2a shows the SEM image of a distinct PCNC. The PhC F−P cavity is a simple silicon waveguide structure etched with 14 ellipse holes. The end coupling structure simplifies the PCNC filter unit as the shape of a waveguide with a 6 μm core length and near 470 nm width. Figure 2b illustrates the operating principle and a variety of adjustable detailed parameters of single PCNC to realize a compact cavity with a finely tunable resonant wavelength. Hx, Hy, a, W, and D are the ellipse hole horizontal axis, vertical axis, period, nanobeam width, and center distance of a PCNC, respectively. The input light of resonant wavelength from one end of the nanobeam will be strongly coupled into the center of the PCNC and coupled out from another end. The input port can receive the light directly from the inner waveguide or from free space by grating couplers [see Figure S2 of Supplement 1], while the mature Ge/Si photodetector could be integrated on the SOI chip to detect the transmitted power of the output port. As a proof-of-concept demonstration, grating couplers are used to couple light into and out of the PCNC. The photonic crystal bandgap of the tapered ellipse holes of PCNC structure is shown in the Figure 2c. The ellipse holes in the schematic with leading lines represents a type of one-dimensional PhC

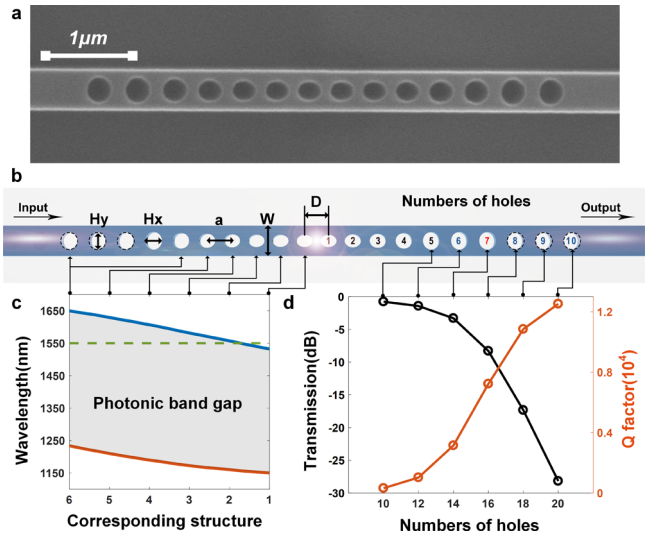

Figure 2. PCNC unit design. (a) SEM image of a PCNC unit. The core length is only 6 μm. (b) Schematic of a PCNC unit. Hx, Hy, a, W, and D are the ellipse hole horizontal axis, vertical axis, period, nanobeam width, and center distance of a PCNC, respectively. The number of holes is a parameter of design. (c) Photonic band gap of tapered one-dimensional photonic crystal structure. (d) Insertion losses in resonant wavelength and Q factors of PCNC structures with different numbers of holes.

consisting of such periodic holes. And, the corresponding blue and red lines are the upper and lower photonic band of the bandgap of this type of PhC. It shows that the light modes with a wavelength near 1550 nm can exist in the central holes but will be reflected by the uniform periodic holes in two ends where the light mode is located in the bandgap. The Bloch mode of the 10 gradually changed holes in between matches the light mode to increase the intrinsic quality factor (Q_i) of this F−P cavity and reduce the leakage of power in the side wall. Therefore, the PCNC units can be arranged closely with negligible crosstalk. The characteristic of single resonance peak in the working wavelength range makes it more convenient to reconstruct the spectrum.

After all the parameters are optimized through the three-dimensional finite difference time-domain (3D-FDTD) iterated simulations with the steepest decent algorithm, we obtained a high Q_i of 2.6×10^5 and a small mode volume of 0.014 μm^3. The detailed design methods and specific parameters are provided in Figure S1 and Table S1 of Supplement 1. The intrinsic and total quality factors Q_i and Q_t can be related to the intrinsic and total loss rates γ_i and $\gamma_t = \gamma_i + \gamma_c$ of the cavity, as $\gamma_i = \omega_0/2Q_i$ and $\gamma_t = \omega_0/2Q_t$, where γ_c is the coupled rate. To simplify the PCNC unit with end coupling structure, we directly cut down the holes number of the PhC mirrors in two ends while keeping the 10 tapered holes structure at the center. As the number of whole holes decrease from 20 to 10 (10 to 5 in each side), the coupled rates γ_c will increase to enhance the light-cavity coupling. The total Q factor will decrease as the relationship between Q_t and γ_t. On the other hand, the insertion loss (IL) of the resonant wavelength will be reduced since the light passes through the cavity by twice light-cavity coupling. Figure 2d reveals the change of IL and Q factor at the resonant wavelengths. Considering both factors, we choose 14 holes as the final PCNC design.

https://doi.org/10.1021/acsphotonics.1c00719
ACS Photonics XXXX, XXX, XXX−XXX

As to the PCNC array, the resonant wavelength of PCNC unit could be tuned by changing the size of the cavity. Figure 3a illustrates that the two parameters of the cavity size,

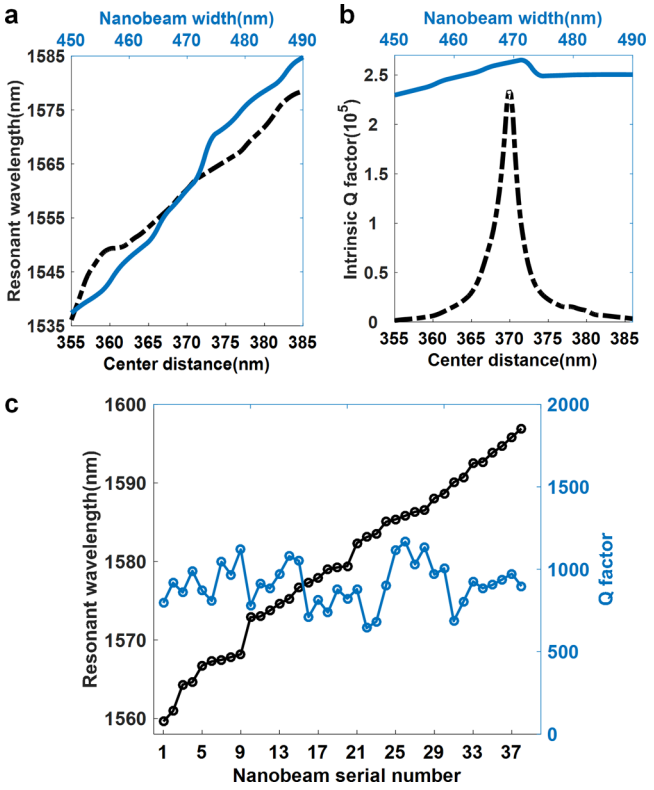

Figure 3. PCNC array design. (a) Resonant wavelength as a function of nanobeam width and center distance of PCNC (W and D in Figure 2b) in blue and black, respectively. (b) Intrinsic Q factor as a function of nanobeam width and center distance of PCNC in blue and black, respectively. (c) Measured results of Q factors and resonant wavelengths of the fabricated 38 PCNC units in blue and black, respectively.

nanobeam width and center distance (W and D in Figure 2b), are nearly linearly related to the resonant wavelength of PCNC. One may see that the rate of change differs between the wavelength shorter and longer than 1570 nm, which can result in an uneven distribution of resonant wavelengths (in Figure 1d) when we use uniform W changes. But thanks to the reconstruction algorithm and the bandwidth of the resonance peak, this difference in uniformity can be allowed to achieve spectral reconstruction. However, the intrinsic Q factor, Q_i will deteriorate rapidly when the center distance shifts from its optimal value due to the breaking of mode match along the nanobeam, as shown in Figure 3b. Fortunately, the Q_i remains high and stable when changing the nanobeam width, ensuring the coherence of transmission spectra. We measured the transmission spectra of all the 38 PCNC units, and the resonant wavelengths and Q factors (Q_i) are shown in Figure 3c. One can see that indeed the resonant wavelengths are increased linearly and the Q factor remains stable with a little fluctuation. Thus, the measured spectra agree well with the theoretic prediction. The average difference of resonant wavelengths between two adjacent PCNC units is 0.9 nm. The overall resonant wavelengths have a red shift, covering the bands from 1560 to 1600 nm, and the measured Q factors are reduced to around 1000, but the fine linear distribution of resonant wavelengths and stable Q factor can meet the requirements of the computational reconstruction method. Even though the overall wavelength range shifts out of our target spectra, the mature thermal-optic microheaters on an SOI chip can be easily utilized to calibrate the resonant wavelengths to the targeted spectra.

RESULTS

Now, we demonstrate the capability to reconstruct the incident-light spectra employing the PCNC spectrometer. The incident light was generated using a broadband optical source across infrared conventional band and long-wavelength band and a programmable optical filter. As a comparison to the reconstruction results of the PCNC spectrometer, shown in Figure 4, the incident light was also directly measured by a commercial benchtop optical spectrum analyzer (OSA, YOKOGAWA AQ6370C). The PCNC spectrometer is able to reproduce all the major shapes of the spectra. Note that the reconstruction spectrum is normalized for the different total losses of two methods to clearly display the deviation of the spectra. The deviations between spectra detected by a commercial OSA and reconstructed by our spectrometer are small in the major component. A high extinction ratio up to 30 dB is realized by the PCNC. In resolving single peak spectra light with 3 and 1 nm bandwidth as shown in Figures 4a,b, the full width at half-maximum (fwhm) (minus 3 dB from peak intensity) of reconstructed spectra is almost equivalent to that of reference and the measured central wavelength is accurate. The ability to distinguish two close spectral peaks is also proven in Figures 4d,e with 10 and 5 nm distance. Ramp spectrum and multiple narrow peak spectrum can also be reconstructed as shown in Figures 4c,e.

The resolution can be further improved by increasing the quantity of PCNC units to measure more samples. More filter units can offer denser resonant wavelength distribution in operating range by shortening step length of parameters or even repeating the same structure. The operation wavelength range can also be extended by more PCNC units, which is not easy for material engineered spectrometers. Benefiting from the compact footprint and flexible structure of PCNC and CMOS technology, a large quantity of different PCNC units can be fabricated on one chip through standard CMOS processes.

GENERALIZED MODULAR SPECTROMETERS

As mentioned above, the spectrometer is an important instrument for spectrum analysis in various scenarios, which means totally different operation spectral bands. In general, one novel prototype of spectrometer is elaborately designed for one specific spectral band. And it would take great efforts and costs to redesign and adapt to another wavelength range, especially for the spectrometers based on the intrinsic spectral response of artificial materials. Thanks to the correlation between the PhC structure scale and the frequency of photonic bands, we can easily transplant the reference PCNC spectrometer to any other spectral bands by scaling all the parameters of nanobeam structures. For example, based on the optimized structure of our PCNC spectrometer and its capability to reconstruct spectrum around 1550 nm wavelength, we further transplant the prototype of this spectrometer to 1310 nm band and 2400 nm band. The former band is another low-loss communication window of fiber-optic communication other than 1550 nm band, and the latter

https://doi.org/10.1021/acsphotonics.1c00719
ACS Photonics XXXX, XXX, XXX−XXX

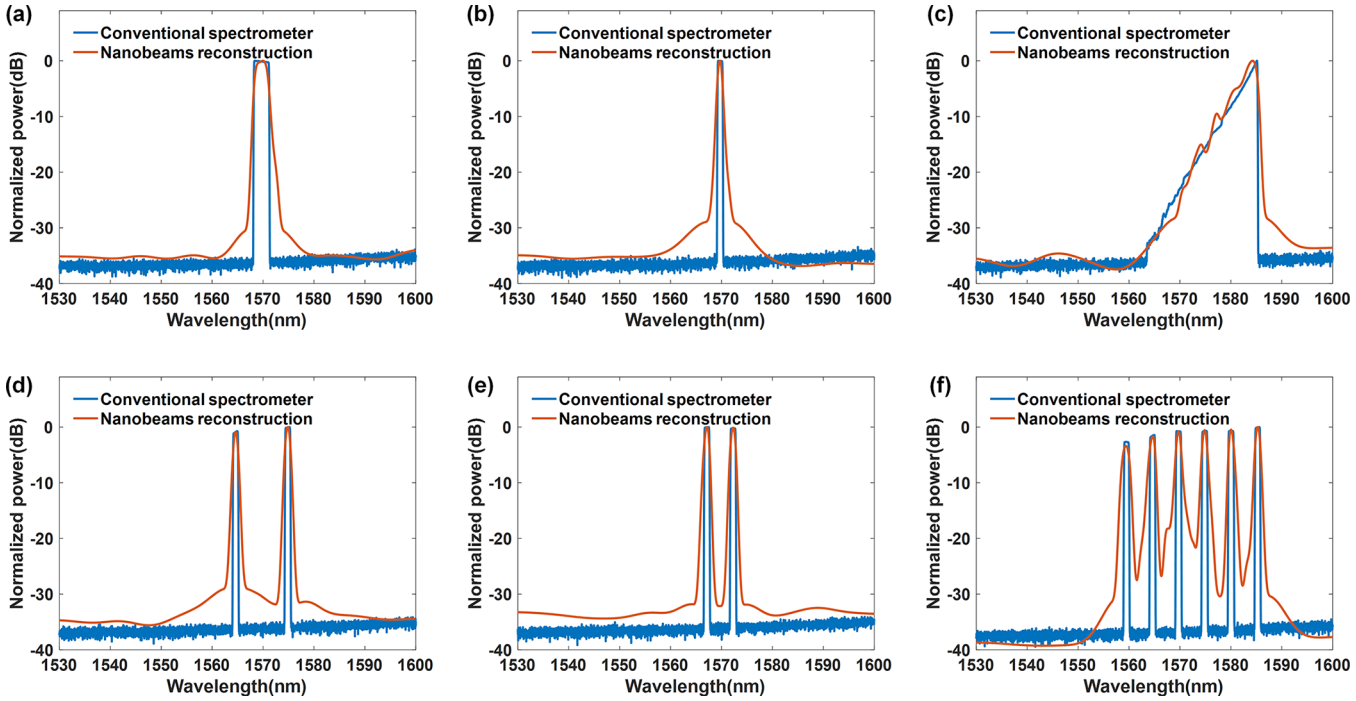

Figure 4. Incident spectra measured by a conventional benchtop spectrometer and computational reconstruction with the PCNC spectrometer as blue and red lines, respectively. (a) 3 nm fwhm single peak spectrum of the incident light. (b) 1 nm fwhm single peak spectrum of the incident light. (c) Broadband incident light with triangular spectrum. (d) Two-peak spectrum of incident light with 10 nm distance. (e) Two-peak spectrum of incident light with 5 nm distance. (f) Broadband incident light with a range of spectral peaks.

aims to the spectroscopic sensing applications with the help of prominent absorption cross sections of the molecules in the mid-infrared band.[33]

The transplant strategy is simply increasing the size of prototype by 1.55 times for 2400 nm band and scaling down the size to 0.85 for 1310 nm band without extra design and optimization, shown as Figure 5a. Then the resonant wavelengths of PCNC array can also be gradually shifted by changing the width of nanobeam. Figure 5b,c show the simulated results of the resonant wavelength and intrinsic *Q* factor of the corresponding PCNC structure for 2400 and 1310 nm, respectively. The linear wavelength tuning and stable *Q* factor are realized due to the universal mechanism of the PCNC spectrometer. As a structure engineered spectrometer, the transplanting ability to farther optical bands would not be hindered by the fabrication platform. For example, the PCNC spectrometer can be realized on a visible-light transparent platform such as S_3N_4 for visible light applications.

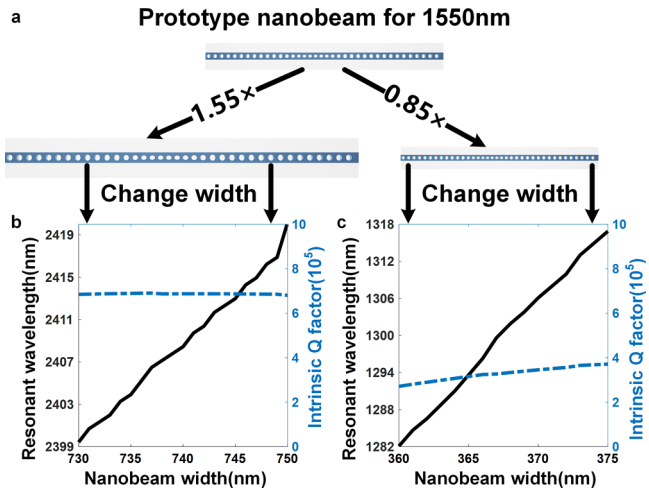

Figure 5. Schematic and results of easy transplant process. (a) Transplanting the prototype PCNC for 1550−2400 and 1310 nm by simply scaling the structure parameters by 2 and 0.85 times. (b) Intrinsic Q factor and resonant wavelength as a function of nanobeam width of PCNC in blue and black, respectively. The resonant wavelength is around 2400 nm. (c) Intrinsic Q factor and resonant wavelength as a function of nanobeam width of PCNC in blue and black, respectively. The resonant wavelength is around 1310 nm.

Considering all these advantages in design and manufacture, the PCNC spectrometer has great potential to be a generalized modular spectrometer that can be easily customized as the varied demands of applications. Figure 6 illustrates the standard customization flow to fast deliver the commercial miniaturized spectrometer products from the PCNC prototype. The design processes start from determining the operation bands of the working scenarios, as the demands of practical applications such as chemical gas characterization and telecom spectrum analysis. The materials of the chosen CMOS platform should be low-loss to the operation bands. The corresponding resonant wavelength of the PCNC is adjusted by scaling and optimizing the structure parameters from prototype structure, as mentioned above. Then, the measurement wavelength range and resolution requirements are taken into consideration together. To meet the requirement of a high resolution, the width change between nanobeams needs to be fine-tuned. Or if the broadband operation range is the primary goal, a relatively large wavelength gradient would be acceptable. Based on the wavelength gradient, a sufficient number of PCNCs are used in the PCNC array to reach the indicators of requirement. After adding the mature receiving interface and photodetector on the layout design, the photonic device can be

https://doi.org/10.1021/acsphotonics.1c00719
ACS Photonics XXXX, XXX, XXX−XXX

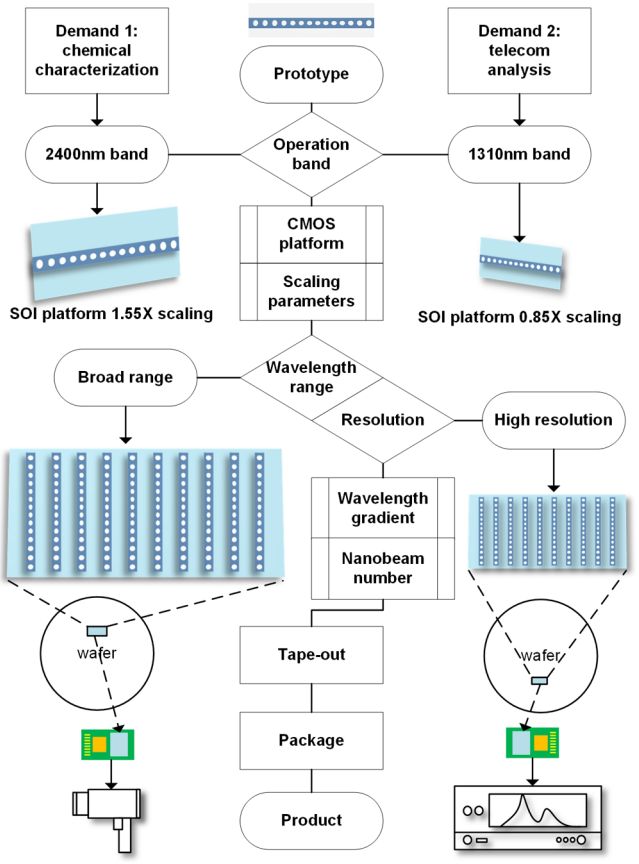

Figure 6. Standard customization flow from proposed PCNC prototype to commercial miniaturized spectrometers. Two types of application demands: chemical gas characterization and telecom spectrum analysis as examples.

fabricated on a wafer through CMOS processes and tape out in large-scale and low-cost. A chip level turn-key solution can be realized by packaging the photonic chip and an application specific integrated circuit (ASIC) with built-in computational reconstruction algorithm. Various types of competitive small spectrometer products can be easily constructed base on these solutions. The agile development processes of the customization flow would make the iteration of products faster and more efficient.

CONCLUSION

In summary, we have demonstrated a compact chip-based spectrometer by combining the complementary advantages of flexible PCNC array structure and computational reconstruction scheme. Using 38 PCNC units with an only 6 μm core length and a 3 μm spacing between units, the spectrometer accurately reconstructs the incident-light spectra around 1580 nm with an extinction ratio up to 30 dB. The employing of computational reconstruction exempts the requirement for high Q factor of the PCNC filter, thus loosening the fabrication process. And the use of CMOS compatible PCNC structure make it easier to be fabricated and integrated in large scale for higher resolution and boarder operating range. Moreover, the structure engineered PCNC spectrometer overcomes the inherent defect of the material based computational spectrometers since it can be easily transplanted to other optical bands, such as around 2400 and 1310 nm. Based on the generalized modular PCNC spectrometer, we illustrate a flexible customization flow to construct various spectrometer products from the proposed PCNC prototype. The compact, scalable and transplantable PCNC spectrometer with low fabrication cost and high yield shows great potential to be widely applied in various spectroscopic applications such as portable chemical characterization, personalized health care and lab-on-a-chip system.

METHODS

Chip Fabrication. We fabricate the PCNC spectrometer on a silicon-on-insulator (SOI) wafer with a 220 nm thick top silicon layer and a 2 μm buried oxide layer. The fabrication of the PCNC spectrometer is very simple with only two steps. First, the PCNC array structure is defined using a single electron-beam lithography exposure. Then, the pattern is transferred to the silicon layer via inductively coupled plasma (ICP) etching. Because of the use of shallow etched grating couplers, other lithography and etching steps are implemented to fabricate the fan-shaped grating couplers in this demonstration. The two grating couplers and one waveguide structures without PCNC etching holes are also fabricated as a comparison. The measured total insertion loss of two side grating couplers and the waveguide is approximately 7 dB.

Characterization and Test. The spectrometer is tested with the signal generated by a combination of a broadband amplified spontaneous emission laser source (ASE laser source) and a programmable optical filter (FINISAR W1000s). The spectral response of each PCNC is predetermined and calibrated before the reconstruction by setting the filter in full-pass status. Then the filter is programmed as six different spectral transmission functions to simulate six typical unknown incident-light spectra that need to be measured. The generated light is received by the PCNC spectrometer through a fiber and grating coupler. The transmitted light power of each PCNC unit is measured with an optical power meter. The obtained data as well as the predetermined spectral responses are used in the algorithm to reconstruct incident spectra. The shaping spectra are also directly measured by a conventional benchtop optical spectrum analyzer (OSA, YOKOGAWA AQ6370C) as a comparison.

ASSOCIATED CONTENT

Supporting Information

The Supporting Information is available free of charge at https://pubs.acs.org/doi/10.1021/acsphotonics.1c00719.

Details of the nanobeam design and spectrum reconstruction (PDF)

AUTHOR INFORMATION

Corresponding Author

Jianji Dong − *Wuhan National Laboratory for Optoelectronics, School of Optical and Electronic Information, Huazhong University of Science and Technology, Wuhan 430 074, China;* orcid.org/0000-0002-1852-8650; Email: jjdong@mail.hust.edu.cn

Authors

Ziwei Cheng − *Wuhan National Laboratory for Optoelectronics, School of Optical and Electronic Information, Huazhong University of Science and Technology, Wuhan 430 074, China*

https://doi.org/10.1021/acsphotonics.1c00719
ACS Photonics XXXX, XXX, XXX−XXX

Yuhe Zhao − *Wuhan National Laboratory for Optoelectronics, School of Optical and Electronic Information, Huazhong University of Science and Technology, Wuhan 430 074, China*
Jiahui Zhang − *Wuhan National Laboratory for Optoelectronics, School of Optical and Electronic Information, Huazhong University of Science and Technology, Wuhan 430 074, China*
Hailong Zhou − *Wuhan National Laboratory for Optoelectronics, School of Optical and Electronic Information, Huazhong University of Science and Technology, Wuhan 430 074, China*
Dingshan Gao − *Wuhan National Laboratory for Optoelectronics, School of Optical and Electronic Information, Huazhong University of Science and Technology, Wuhan 430 074, China*
Xinliang Zhang − *Wuhan National Laboratory for Optoelectronics, School of Optical and Electronic Information, Huazhong University of Science and Technology, Wuhan 430 074, China*

Complete contact information is available at: https://pubs.acs.org/10.1021/acsphotonics.1c00719

Notes

The authors declare no competing financial interest.

■ ACKNOWLEDGMENTS

The authors acknowledge the funding provided by the National Natural Science Foundation of China (62075075, 61805090).

■ REFERENCES

(1) Savage, N. Spectrometers. *Nat. Photonics* **2009**, *3*, 601−602.
(2) Blind, N.; Le Coarer, E.; Kern, P.; Gousset, S. Spectrographs for astrophotonics. *Opt. Express* **2017**, *25*, 27341−27369.
(3) Harris, A. T. Spectral mapping tools from the earth sciences applied to spectral microscopy data. *Cytometry, Part A* **2006**, *69*, 872−9.
(4) Mulla, D. J. Twenty five years of remote sensing in precision agriculture: Key advances and remaining knowledge gaps. *Biosystems Eng.* **2013**, *114*, 358−371.
(5) Zheng, S. N.; Zou, J.; Cai, H.; Song, J. F.; Chin, L. K.; Liu, P. Y.; Lin, Z. P.; Kwong, D. L.; Liu, A. Q. Microring resonator-assisted Fourier transform spectrometer with enhanced resolution and large bandwidth in single chip solution. *Nat. Commun.* **2019**, *10*, 2349.
(6) Yang, Z.; Albrow-Owen, T.; Cai, W.; Hasan, T. Miniaturization of optical spectrometers. *Science* **2021**, *371*, 6528.
(7) Wolffenbuttel, R. F. State-of-the-Art in Integrated Optical Microspectrometers. *IEEE Trans. Instrum. Meas.* **2004**, *53*, 197−202.
(8) Bacon, C. P.; Mattley, Y.; DeFrece, R. Miniature spectroscopic instrumentation: Applications to biology and chemistry. *Rev. Sci. Instrum.* **2004**, *75*, 1−16.
(9) DeCorby, R. G.; Ponnampalam, N.; Epp, E.; Allen, T.; McMullin, J. N. Chip-scale spectrometry based on tapered hollow Bragg waveguides. *Opt. Express* **2009**, *17*, 16632−45.
(10) Kita, D. M.; Miranda, B.; Favela, D.; Bono, D.; Michon, J.; Lin, H.; Gu, T.; Hu, J. High-performance and scalable on-chip digital Fourier transform spectroscopy. *Nat. Commun.* **2018**, *9*, 4405.
(11) Peroz, C.; Calo, C.; Goltsov, A.; Dhuey, S.; Koshelev, A.; Sasorov, P.; Ivonin, I.; Babin, S.; Cabrini, S.; Yankov, V. Multiband wavelength demultiplexer based on digital planar holography for on-chip spectroscopy applications. *Opt. Lett.* **2012**, *37*, 695−7.
(12) Redding, B.; Fatt Liew, S.; Bromberg, Y.; Sarma, R.; Cao, H. Evanescently coupled multimode spiral spectrometer. *Optica* **2016**, *3*, 956−962.
(13) Souza, M.; Grieco, A.; Frateschi, N. C.; Fainman, Y. Fourier transform spectrometer on silicon with thermo-optic non-linearity and dispersion correction. *Nat. Commun.* **2018**, *9*, 665.
(14) Stender, A. S.; Marchuk, K.; Liu, C.; Sander, S.; Meyer, M. W.; Smith, E. A.; Neupane, B.; Wang, G.; Li, J.; Cheng, J. X.; Huang, B.; Fang, N. Single cell optical imaging and spectroscopy. *Chem. Rev.* **2013**, *113*, 2469−527.
(15) Wan, N. H.; Meng, F.; Schroder, T.; Shiue, R. J.; Chen, E. H.; Englund, D. High-resolution optical spectroscopy using multimode interference in a compact tapered fibre. *Nat. Commun.* **2015**, *6*, 7762.
(16) Yang, T.; Xu, C.; Ho, H. P.; Zhu, Y. Y.; Hong, X. H.; Wang, Q. J.; Chen, Y. C.; Li, X. A.; Zhou, X. H.; Yi, M. D.; Huang, W. Miniature spectrometer based on diffraction in a dispersive hole array. *Opt. Lett.* **2015**, *40*, 3217−20.
(17) Wang, S. W.; Xia, C.; Chen, X.; Lu, W.; Li, M.; Wang, H.; Zheng, W.; Zhang, T. Concept of a high-resolution miniature spectrometer using an integrated filter array. *Opt. Lett.* **2007**, *32*, 632−4.
(18) Xia, Z.; Eftekhar, A. A.; Soltani, M.; Momeni, B.; Li, Q.; Chamanzar, M.; Yegnanarayanan, S.; Adibi, A. High resolution on-chip spectroscopy based on miniaturized microdonut resonators. *Opt. Express* **2011**, *19*, 12356−64.
(19) Emadi, A.; Wu, H.; de Graaf, G.; Wolffenbuttel, R. Design and implementation of a sub-nm resolution microspectrometer based on a Linear-Variable Optical Filter. *Opt. Express* **2012**, *20*, 489−507.
(20) Florjanczyk, M.; Cheben, P.; Janz, S.; Scott, A.; Solheim, B.; Xu, D. X. Multiaperture planar waveguide spectrometer formed by arrayed Mach-Zehnder interferometers. *Opt. Express* **2007**, *15*, 18176−89.
(21) Meng, J.; Cadusch, J. J.; Crozier, K. B. Detector-Only Spectrometer Based on Structurally Colored Silicon Nanowires and a Reconstruction Algorithm. *Nano Lett.* **2020**, *20*, 320−328.
(22) Momeni, B.; Hosseini, E. S.; Adibi, A. Planar photonic crystal microspectrometers in silicon-nitride for the visible range. *Opt. Express* **2009**, *17*, 17060−9.
(23) Momeni, B.; Hosseini, E. S.; Askari, M.; Soltani, M.; Adibi, A. Integrated photonic crystal spectrometers for sensing applications. *Opt. Commun.* **2009**, *282*, 3168−3171.
(24) Muneeb, M.; Vasiliev, A.; Ruocco, A.; Malik, A.; Chen, H.; Nedeljkovic, M.; Penades, J. S.; Cerutti, L.; Rodriguez, J. B.; Mashanovich, G. Z.; Smit, M. K.; Tourni, E.; Roelkens, G. III-V-on-silicon integrated micro - spectrometer for the 3 mum wavelength range. *Opt. Express* **2016**, *24*, 9465−72.
(25) Yang, T.; Li, C.; Wang, Z.; Ho, H. An ultra compact spectrometer based on the optical transmission through a micro interferometer array. *Optik* **2013**, *124*, 1377−1385.
(26) Schweiger, G.; Nett, R.; Weigel, T. Microresonator array for high-resolution spectroscopy. *Opt. Lett.* **2007**, *32*, 2644−2646.
(27) Kyotoku, B. B.; Chen, L.; Lipson, M. Sub-nm resolution cavity enhanced microspectrometer. *Opt. Express* **2010**, *18*, 102−7.
(28) Song, J.; Zhu, N. Design and fabrication of compact etched diffraction grating demultiplexers based on -Si nanowire technology. *Electron. Lett.* **2008**, *44*, 816−818.
(29) Ryckeboer, E.; Gassenq, A.; Muneeb, M.; Hattasan, N.; Pathak, S.; Cerutti, L.; Rodriguez, J. B.; Tournie, E.; Bogaerts, W.; Baets, R.; Roelkens, G. Silicon-on-insulator spectrometers with integrated GaInAsSb photodiodes for wide-band spectroscopy from 1510 to 2300 nm. *Opt. Express* **2013**, *21*, 6101−8.
(30) Cheben, P.; Schmid, J. H.; Delage, A.; Densmore, A.; Janz, S.; Lamontagne, B.; Lapointe, J.; Post, E.; Waldron, P.; Xu, D. X. A high-resolution silicon-on-insulator arrayed waveguide grating micro-spectrometer with sub-micrometer aperture waveguides. *Opt. Express* **2007**, *15*, 2299−306.
(31) Cheng, R.; Zou, C. L.; Guo, X.; Wang, S.; Han, X.; Tang, H. X. Broadband on-chip single-photon spectrometer. *Nat. Commun.* **2019**, *10*, 4104.
(32) Malik, A.; Muneeb, M.; Shimura, Y.; Van Campenhout, J.; Loo, R.; Roelkens, G. Germanium-on-silicon planar concave grating wavelength (de)multiplexers in the mid-infrared. *Appl. Phys. Lett.* **2013**, *103*, 161119.

(33) Muneeb, M.; Chen, X.; Verheyen, P.; Lepage, G.; Pathak, S.; Ryckeboer, E.; Malik, A.; Kuyken, B.; Nedeljkovic, M.; Van Campenhout, J.; Mashanovich, G. Z.; Roelkens, G. Demonstration of Silicon-on-insulator mid-infrared spectrometers operating at 3.8 mum. *Opt. Express* **2013**, *21*, 11659−69.
(34) Vasiliev, A.; Muneeb, M.; Allaert, J.; Van Campenhout, J.; Baets, R.; Roelkens, G. Integrated Silicon-on-Insulator Spectrometer With Single Pixel Readout for Mid-Infrared Spectroscopy. *IEEE J. Sel. Top. Quantum Electron.* **2018**, *24*, 1−7.
(35) Nitkowski, A.; Chen, L.; Lipson, M. Cavity-enhanced on-chip absorption spectroscopy using microring resonators. *Opt. Express* **2008**, *16*, 11930−6.
(36) Chen, Y.; Lin, H.; Hu, J.; Li, M. Heterogeneously integrated silicon photonics for the mid-infrared and spectroscopic sensing. *ACS Nano* **2014**, *8*, 6955−61.
(37) Zheng, S.; Cai, H.; Song, J.; Zou, J.; Liu, P. Y.; Lin, Z.; Kwong, D.-L.; Liu, A.-Q. A Single-Chip Integrated Spectrometer via Tunable Microring Resonator Array. *IEEE Photonics J.* **2019**, *11*, 1−9.
(38) Nozaki, K.; Tanabe, T.; Shinya, A.; Matsuo, S.; Sato, T.; Taniyama, H.; Notomi, M. Sub-femtojoule all-optical switching using a photonic-crystal nanocavity. *Nat. Photonics* **2010**, *4*, 477−483.
(39) Gan, X.; Pervez, N.; Kymissis, I.; Hatami, F.; Englund, D. A high-resolution spectrometer based on a compact planar two dimensional photonic crystal cavity array. *Appl. Phys. Lett.* **2012**, *100*, 231104.
(40) Pervez, N. K.; Cheng, W.; Jia, Z.; Cox, M. P.; Edrees, H. M.; Kymissis, I. Photonic crystal spectrometer. *Opt. Express* **2010**, *18*, 8277−85.
(41) Liapis, A. C.; Gao, B.; Siddiqui, M. R.; Shi, Z.; Boyd, R. W. On-chip spectroscopy with thermally tuned high-Q photonic crystal cavities. *Appl. Phys. Lett.* **2016**, *108*, 021105.
(42) Wang, Z.; Yi, S.; Chen, A.; Zhou, M.; Luk, T. S.; James, A.; Nogan, J.; Ross, W.; Joe, G.; Shahsafi, A.; Wang, K. X.; Kats, M. A.; Yu, Z. Single-shot on-chip spectral sensors based on photonic crystal slabs. *Nat. Commun.* **2019**, *10*, 1020.
(43) Zhu, Y.; Lei, X.; Wang, K. X.; Yu, Z. Compact CMOS spectral sensor for the visible spectrum. *Photonics Res.* **2019**, *7*, 961−966.
(44) Johnson, S.G.; Mekis, A.; Fan, S.; Joannopoulos, J.D. Molding the flow of light. *Comput. Sci. Eng.* **2001**, *3*, 38−47.
(45) Zhang, W.; Serna, S.; Le Roux, X.; Vivien, L.; Cassan, E. Silicon nanobeam cavity for ultra-localized light-matter interaction. *Opt. Lett.* **2017**, *42*, 3323−3326.
(46) Li, T.; Gao, D.; Zhang, D.; Cassan, E. High- Q and High-Sensitivity One-Dimensional Photonic Crystal Slot Nanobeam Cavity Sensors. *IEEE Photonics Technol. Lett.* **2016**, *28*, 689−692.
(47) Li, E.; Gao, Q.; Chen, R. T.; Wang, A. X. Ultracompact Silicon-Conductive Oxide Nanocavity Modulator with 0.02 Lambda-Cubic Active Volume. *Nano Lett.* **2018**, *18*, 1075−1081. PMID: 29309164
(48) Huang, Z.; Cui, K.; Li, Y.; Feng, X.; Liu, F.; Zhang, W.; Huang, Y. Strong Optomechanical Coupling in Nanobeam Cavities based on Hetero Optomechanical Crystals. *Sci. Rep.* **2015**, *5*, 15964.
(49) Deotare, P. B.; Kogos, L. C.; Bulu, I.; Loncar, M. Photonic Crystal Nanobeam Cavities for Tunable Filter and Router Applications. *IEEE J. Sel. Top. Quantum Electron.* **2013**, *19*, 3600210−3600210.
(50) Cheng, Z.; Dong, J.; Zhang, X. Ultracompact optical switch using a single semisymmetric Fano nanobeam cavity. *Opt. Lett.* **2020**, *45*, 2363−2366.
(51) Kurokawa, U.; Choi, B. I.; Chang, C.-C. Filter-Based Miniature Spectrometers: Spectrum Reconstruction Using Adaptive Regularization. *IEEE Sens. J.* **2011**, *11*, 1556−1563.
(52) Wang, P.; Menon, R. Computational spectrometer based on a broadband diffractive optic. *Opt. Express* **2014**, *22*, 14575−87.
(53) Redding, B.; Liew, S. F.; Sarma, R.; Cao, H. Compact spectrometer based on a disordered photonic chip. *Nat. Photonics* **2013**, *7*, 746−751.
(54) Bao, J.; Bawendi, M. G. A colloidal quantum dot spectrometer. *Nature* **2015**, *523*, 67−70.
(55) Zhu, X.; Bian, L.; Fu, H.; Wang, L.; Zou, B.; Dai, Q.; Zhang, J.; Zhong, H. Broadband perovskite quantum dot spectrometer beyond human visual resolution. *Light: Sci. Appl.* **2020**, *9*, 73.
(56) Yang, Z.; et al. Single-nanowire spectrometers. *Science* **2019**, *365*, 1017−1020.
(57) Chang, C. C.; Lee, H. N. On the estimation of target spectrum for filter-array based spectrometers. *Opt. Express* **2008**, *16*, 1056−61.
(58) Hansen, P. C. Rank-Deficient and Discrete Ill-Posed Problems: Numerical Aspects of Linear Inversion. *SIAM* **1998**, *4*, 1.
(59) Atabaki, A. H.; et al. Integrating photonics with silicon nanoelectronics for the next generation of systems on a chip. *Nature* **2018**, *556*, 349−354.

https://doi.org/10.1021/acsphotonics.1c00719
ACS Photonics XXXX, XXX, XXX−XXX